

Cascaded coherent Raman scattering by phonon polaritons

G. Kh. Kitaeva,* K. A. Kuznetsov, A. A. Mikhailovsky and A. N. Penin

Department of Physics, Moscow State University, 119899 Moscow, Russia

We consider the cascaded part of coherent four-wave Raman scattering in crystals without inversion symmetry as a method of spectroscopy of phonon polaritons. The theory of this effect is developed accounting for the limited dimensions of the scattering area and imaginary character of the non-linear susceptibilities. The experimental results for four-wave cascaded scattering by polaritons in crystals of LiIO_3 , $\text{LiNbO}_3:\text{Mg}$ and $\text{LiNbO}_3:\text{Mg}:\text{Nd}$ are presented. The effect of narrowing of the polariton lineshape is observed in doped LiNbO_3 in the region of strong polariton absorption. The probable nature of the narrowing, connected with the excitation of the electronic states during the four-wave mixing, is discussed. Copyright © 2000 John Wiley & Sons, Ltd.

INTRODUCTION

The dispersion characteristics of phonon polaritons are directly related to phonon parameters, such as frequencies, damping constants and oscillator strengths. Owing to the strong dependence on the phonon oscillator strength, polariton dispersion is extremely sensitive to various small changes in the medium composition or structure. Weak second-order or impurity polar phonon resonance can be observed in polariton spectra rather than in Raman spectra.¹ Usually polariton dispersion in crystals without inversion symmetry is studied in the scheme of the near-forward Raman scattering. Most of the scattered light intensity is provided by the second-order susceptibility $\chi^{(2)}$ in this scheme. As distinct from IR spectroscopy, this method does not require an IR technique and enables to exclude surface effects. However, its application is often limited because of the low intensity of the scattered radiation, especially when small-sized crystal areas are studied. The time-resolved study of the dynamics of phonon polaritons turns out to be a very good probe of polariton properties.² However, in the impulsive stimulated Raman scattering technique, low-frequency (<5 THz) polaritons can only be studied with an appropriate signal-to-noise ratio.³ This problem can be solved by means of active four-wave mixing spectroscopy.⁴

In a medium without inversion symmetry, in addition to the well-known direct coherent scattering, cascaded scattering can take place in the same optical scheme. The direct coherent scattering arises due to the third-order susceptibility $\chi^{(3)}$ of a medium, and the cascaded wave interaction consists of the two subsequent frequency conversion processes, so that its efficiency is proportional to the square of the second-order susceptibility $\chi^{(2)}$. When the intermediate state is in resonance with the phonon

polariton, and the dispersion characteristics of all other waves are known, this effect can be used as a method for polariton investigation.

The first work on coherent four-wave scattering by polaritons in a medium without inversion symmetry was performed in the 1960s;⁵ in the 1970s, most studies were dedicated to the analysis of the interference of direct and cascaded four-wave mixing processes and the investigation of the cubic non-linear susceptibility $\chi^{(3)}$ dispersion.^{6–10} Now the effect of cascaded four-wave scattering has been successfully used in time- and space-resolved studies of polaritons.^{11,12} In this paper, we consider stationary coherent four-wave Raman scattering.^{13,14} In the case of the frequency–wavevector domain scheme, the dependence of the signal intensity on the wave mismatches contains information about polariton dispersion and absorption characteristics. In all previous theoretical studies, the scattering medium was regarded as homogeneous and large enough to satisfy the condition when the linear dimensions l of the scattering object are much larger than the polariton free path: $l\alpha_p \gg 1$, α_p being the polariton absorption coefficient. Also, it was implied that the scattered element could be regarded as an infinite plane layer.¹⁰ In this work, first, we extend the conventional theoretical model for the cases when the sizes of the scattering area are not very large in comparison with the polariton free path and are bounded in all three directions. Second, we depict the procedure of receiving and processing of experimental results, and finally discuss the results obtained for a crystal of LiIO_3 and crystals of LiNbO_3 doped with Mg and Nd.

THEORY

Suppose that three pump waves enter the medium (Fig. 1), and their fields are expressed as

$$\mathbf{E}_i = \mathbf{E}_{i0}(\mathbf{r}) \exp(-i\omega_i t + i\mathbf{k}_i \mathbf{r}) \quad (1)$$

where i can be 1, 2 or L . The non-linear interaction between \mathbf{E}_1 and \mathbf{E}_2 generates polarization at a difference

* Correspondence to: G. Kh. Kitaeva, Department of Physics, Moscow State University, 119899 Moscow, Russia; e-mail: postmast@qopt.ilc.msu.su

Contract/grant sponsor: Russian Foundation for Basic Research; Contract/grant number: 98-02-16877; Contract/grant number: 99-02-16418.

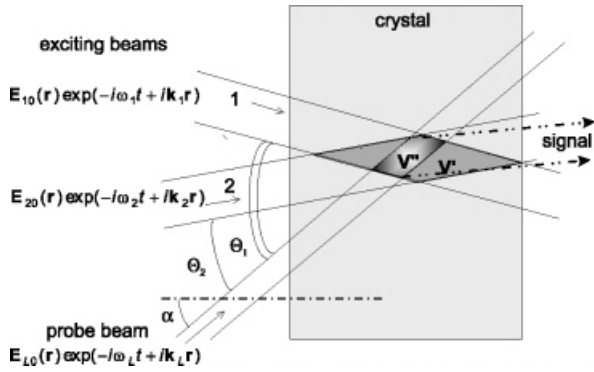


Figure 1. Scheme for coherent four-wave scattering in a crystal without inversion symmetry.

frequency:

$$P^{(1)}(\mathbf{r}, \omega_1 - \omega_2) = \chi_1^{(2)}(\mathbf{r}) E_{10}(\mathbf{r}) E_{20}^*(\mathbf{r}) e^{-i(\omega_1 - \omega_2)t + i(\mathbf{k}_1 - \mathbf{k}_2) \cdot \mathbf{r}} \quad (2)$$

which can be in resonance with the phonon polariton at the frequency ω_p when

$$\omega_1 - \omega_2 = \omega_p \quad (3)$$

$\chi_1^{(2)}$ is the effective value of the second-order susceptibility of the medium for this process. The spatial Fourier components $\mathbf{P}^{(1)}(\mathbf{k}, \omega_p)$ and $\mathbf{E}(\mathbf{r}, \omega_p)$ of the polarization $\mathbf{P}^{(1)}(\mathbf{r}, \omega_p)$ and field $\mathbf{E}(\mathbf{r}, \omega_p)$, generated by this polarization, are related through the polariton Green's function $\mathbf{G}(\mathbf{k}, \omega_p)$.¹⁵

$$\mathbf{E}(\mathbf{k}, \omega_p) = \mathbf{G}(\mathbf{k}, \omega_p) P^{(1)}(\mathbf{k}, \omega_p) \quad (4)$$

A general expression for the polariton Green's function $\mathbf{G}(\mathbf{k}, \omega_p)$ was derived by Klyshko,⁹ accounting for anisotropy of the crystal medium. In the case of ordinary polariton waves, the Green's function is equal to

$$\mathbf{G}(\mathbf{k}, \omega_p) = \frac{\omega_p^2}{c^2} \frac{4\pi}{k^2 - K_p^2(\omega_p)} \quad (5)$$

where $K_p(\omega_p) = k_p + i\alpha_p/2$ is the complex wavevector of the polariton state at frequency ω_p , $k_p = n_p \omega_p / c$, n_p is an ordinary refractive index and α_p is the absorption coefficient of a crystal at the polariton frequency ω_p . Hence we derive

$$\mathbf{E}(\mathbf{r}, \omega_p) = \frac{\chi^{(2)} E_{10} E_{20}^* e^{-i\omega_p t}}{(2\pi)^3} \int d\mathbf{k} \mathbf{G}(\mathbf{k}, \omega_p) e^{i\mathbf{k} \cdot \mathbf{r}} \int_{V'} d\mathbf{r}' e^{i\Delta\mathbf{k}^{(1)} \cdot \mathbf{r}'} \quad (6)$$

where $\Delta\mathbf{k}^{(1)} = \mathbf{k}_1 - \mathbf{k}_2 - \mathbf{k}$. The domain of integration over the wavevectors \mathbf{k} contains all possible magnitudes and alignments of \mathbf{k} . The space integration is made over the volume V' , where wave amplitudes and non-linear susceptibility are non-zero (Fig. 1). The sizes of this area can be limited owing to the small dimensions of the non-linear medium itself, or owing to the finite dimensions of that region inside the crystal, where the pumping beams intersect each other. Here and in what follows we neglect the spatial profiles of pumping beams and distribution of $\chi(\mathbf{r})$ inside the area V' .

In the second stage, the field $\mathbf{E}(\mathbf{r}, \omega_p)$ described by Eqn (6) and the probe pumping wave \mathbf{E}_L are mixed. As a result, the expression for the polarization oscillating at the Stokes frequency

$$\omega_s = \omega_L - \omega_p \quad (7)$$

takes the form

$$\mathbf{P}_{\text{casc}}^{(2)}(\mathbf{r}, \omega_L - \omega_p) = \frac{\chi_1^{(2)*} \chi_2^{(2)} \mathbf{E}_{L0} \mathbf{E}_{10} \mathbf{E}_{20} e^{-i\omega_s t + i\mathbf{k}_s \cdot \mathbf{r}}}{(2\pi)^3} \times \int d\mathbf{k} e^{i\Delta\mathbf{k}^{(2)} \cdot \mathbf{r}} \mathbf{G}(\mathbf{k}, \omega_p) \int_{V'} d\mathbf{r}' e^{-i\Delta\mathbf{k}^{(1)} \cdot \mathbf{r}'} \quad (8)$$

where $\Delta\mathbf{k}^{(2)} = \mathbf{k}_L - \mathbf{k}_s - \mathbf{k}$. Effective values of the second-order susceptibility at the first stage of the cascaded interaction [$\chi_1^{(2)}$] and at the second stage [$\chi_2^{(2)}$] can differ owing to dispersion and anisotropy. To obtain the total polarization at frequency ω_s , one has to account for direct interaction due to $\chi^{(3)}$. Finally, the general expression for the signal intensity dependence from the mismatches takes the form

$$I_s \sim \left| \chi^{(3)} f''(\Delta\mathbf{k}) + \frac{\chi_1^{(2)*} \chi_2^{(2)}}{(2\pi)^3} \int G^*(\mathbf{k}, \omega_p) \times f'^*(\mathbf{q}_1 - \mathbf{k}) f''(\mathbf{q}_2 - \mathbf{k}) d\mathbf{k} \right|^2 \quad (9)$$

where

$$\mathbf{q}_1 \equiv \mathbf{k}_1 - \mathbf{k}_2, \quad \mathbf{q}_2 \equiv \mathbf{k}_L - \mathbf{k}_s, \quad \Delta\mathbf{k} \equiv \mathbf{q}_2 - \mathbf{q}_1 \quad (10)$$

and $f(\mathbf{k})$ is a function dependent on the shape and sizes of the scattering area; for any given vector ξ :

$$f(\vec{\xi}) \equiv \int_V \exp(i\vec{\xi} \cdot \mathbf{r}) d\mathbf{r} \quad (11)$$

For example, when the scattering element has the shape of a rectangular parallelepiped with sides a , b and c , $f(\Delta\mathbf{k})$ is given by

$$f(\Delta\mathbf{k}) = V \frac{\sin(\Delta k_x a/2)}{\Delta k_x a/2} \frac{\sin(\Delta k_y b/2)}{\Delta k_y b/2} \frac{\sin(\Delta k_z c/2)}{\Delta k_z c/2} \quad (12)$$

where Δk_x , Δk_y and Δk_z are the coordinates of the vector mismatch $\Delta\mathbf{k}$. For a spherical element of the radius l , it is given by

$$f(\Delta\mathbf{k}) = 3V \frac{\sin(\Delta kl) - \Delta kl \cos(\Delta kl)}{(\Delta kl)^3} \quad (13)$$

To be precise, one must calculate functions $f'(\mathbf{q}_1 - \mathbf{k})$ and $f''(\mathbf{q}_2 - \mathbf{k})$ in Eqn (9) according to Eqn (11) by integrating over different regions V' and V'' . The last region V'' is the part of V' where the probe pumping wave exists (Fig. 1).

Now let us consider the most common case when the scattering elements V' and V'' have complex shapes but

their linear dimensions (of order of l) are sufficiently large to satisfy the condition

$$\alpha_p l \gg 1 \quad (14)$$

Then the polariton Green's function can be taken outside the integration sign in Eqn (9), since it changes slowly in comparison with the f' and f'' functions. Integration of the residual f' and f'' functions for cubic scattering elements $V' \approx V''$ gives

$$\int f'^*(\mathbf{q}_1 - \mathbf{k}) f''(\mathbf{q}_2 - \mathbf{k}) d\mathbf{k} = (2\pi)^3 f''(\mathbf{q}_2 - \mathbf{q}_1) \quad (15)$$

This seems to be valid for more complicated shapes of scattering elements also. Actually, the shape of scattering element should not affect strongly the signal intensity distribution when conditions in Eqn (14) are true. Substituting Eqn (15) into the general expression of Eqn (9) we obtain for the case of a large scattering element

$$I_s \sim |\chi_{\text{eff}}^{(3)}|^2 |f''(\Delta\mathbf{k})|^2, \quad (16)$$

$$\chi_{\text{eff}}^{(3)} \equiv \chi^{(3)} + \chi_1^{(2)*} \chi_2^{(2)} G^*(\mathbf{q}_1, \omega_p)$$

The same calculation scheme is valid in the case of anti-Stokes coherent scattering ($\omega_s = \omega_L + \omega_p$), or when the cascade process proceeds due to an intermediate resonance with the certain exciton-like medium state at sum frequency $\omega_1 + \omega_2 = \omega_p$ [obviously, Eqns (10) have to be verified according to frequency relationships].

The generalized third-order susceptibility $\chi_{\text{eff}}^{(3)}$ in Eqn (16) contains the cascaded part $\chi_{\text{casc}}^{(3)} \equiv G^*(\mathbf{q}_1, \omega_p) \chi_1^{(2)*} \chi_2^{(2)}$. This term describes the polariton properties. The information on polariton properties at a given frequency ω_p is included in the $\chi_{\text{eff}}^{(3)}$ dependence on the wave mismatch $\tau_p \equiv \mathbf{q}_1 - \mathbf{k}_p$. To obtain it one has to measure the dependence $I_s(\tau_p)$ of the scattered intensity on the polariton phase mismatch τ_p under the condition $\Delta\mathbf{k} = 0$, i.e. when the direct four-wave interaction is mismatched. For o -polarized polaritons the Green's function $\mathbf{G}(\mathbf{k}_1 - \mathbf{k}_2, \omega_p)$ is described by Eqn (5). $\mathbf{G}(\mathbf{k}_1 - \mathbf{k}_2, \omega_p)$ depends on the scalar mismatch $\tau_p = |\mathbf{k}_1 - \mathbf{k}_2| - k_p$ and polariton absorption α_p . Under the realistic conditions $k_p \gg \alpha_p$, $k_p \gg \tau_p$, thus,

$$\mathbf{G}(\mathbf{k}, \omega_p) = \frac{2\pi\omega_p}{n_{pc}} \frac{\tau_p + i\alpha_p/2}{\tau_p^2 + (\alpha_p/2)^2} \quad (17)$$

Substituting Eqn (17) into Eqn (16), we obtain the line-shape of $I_s(\tau_p, \Delta\mathbf{k})$ in the case of large coincident scattering elements, o -polarized polaritons and real $\chi_1^{(2)}$, $\chi_2^{(2)}$, $\chi^{(3)}$:

$$I_s \sim \left\{ [\eta\chi^{(3)}]^2 + \frac{2\eta\chi_1^{(2)}\chi_2^{(2)}\chi^{(3)}\tau_p}{(\alpha_p/2)^2 + \tau_p^2} + \frac{[\chi_1^{(2)}\chi_2^{(2)}]^2}{(\alpha_p/2)^2 + \tau_p^2} \right\} |f''(\Delta\mathbf{k})|^2 \quad (18)$$

where $\eta = n_{pc}/2\pi\omega_p$. The last expression describes the frequency dependence of I_s through dispersion characteristics of second- and third-order susceptibilities, coefficient η and wave mismatches τ_p , $\Delta\mathbf{k}$. The last ones assign the pure angle dependence of I_s at a fixed polariton frequency.

The first term in braces describes the direct four-wave interaction, the last term the pure cascaded part of scattering and the intermediate term the interference between the direct and cascaded processes. When the second-order susceptibilities $\chi_i^{(2)}$ are zero or vanishingly small, the scattering has a pure direct character and $I_s \sim |\chi^{(3)} f''(\Delta\mathbf{k})|^2$, as follows from Eqn (16). It remains the same even if $\chi_i^{(2)}$ are sufficiently large, but the polariton wave mismatch is also large ($\tau_p \gg \alpha_p$) and the last two terms in braces in Eqn (18) are negligible. The intensity of the direct scattering does not depend on τ_p ; it is necessary to provide the four-wave phase matching condition $\Delta\mathbf{k} = 0$ to obtain the peak signal intensity at a given frequency. Tuning the signal frequency synchronously with the frequency of any one pumping wave, one can measure the spectral dependence of $\chi^{(3)}$. However, when $\chi_i^{(2)}$ are non-zero and the polariton wave mismatch is small, the presence of cascaded scattering changes the total angular and spectral distribution of the scattered light according to Eqn (18). Thus, a separation between direct, cascaded and interference parts can be done by analyzing the intensity dependence on τ_p at constant $\Delta\mathbf{k}$. The optimal conditions are when $\Delta\mathbf{k} = 0$ and the signal frequency remains constant. Then the direct scattering gives a constant background which does not change with τ_p , and it can be easily measured at large τ_p . When the contribution of the direct four-wave interaction is much smaller than that of cascaded processes, $I_s(\tau_p)$ has a Lorentzian form. By measuring the position of its peak one can estimate the real parts of the polariton wavevector and the crystal dielectric constant; k_p and ϵ'_p , at the polariton frequency ω_p . The polariton absorption coefficient α_p and the imaginary part of the dielectric constant ϵ''_p can be determined by measuring the half-width of a Lorentzian peak. When the direct and cascaded contributions are comparable, their interference forms an intensity distribution $I_s(\tau_p)$ similar to a Fano-type pattern. Analysis of the $I_s(\tau_p)$ distribution provides the measurement of the ratio $\chi^{(3)}/\chi_1^{(2)}\chi_2^{(2)}$ and the sign of $\chi^{(2)}$.⁶⁻⁸

Equation (18) was obtained earlier¹⁰ for coincident scattering elements in the form of an infinite plane layer. However, in this case the value of η is not the same. η depends on the angle θ_p between the polariton wavevector \mathbf{k}_p and the normal to a layer through the additional multiplier factor $\cos\theta_p$. This difference between the cases of infinite and finite dimensions of the scattering elements is important in the measurement of the relative values of the third- and second-order susceptibilities through the ratio of the direct and cascaded parts of the coherent four-wave scattering. Derived above, Eqn (18) is valid for scattering elements when these are large [Eqn (14)], but finite. They are more appropriate for the interpretation of data obtained under realistic experimental conditions.

The assumption of real susceptibilities $\chi_1^{(2)}$, $\chi_2^{(2)}$, $\chi^{(3)}$ is valid when all frequencies are far from resonances of the scattering medium. Otherwise, the imaginary parts of the susceptibilities should be taken into account. It is impossible, for example, when the interval between the polariton ω_p and a phonon frequency is of the order of the phonon damping constant. Now suppose that

$$\chi_i^{(2)} = \chi_i^{(2')} + i\chi_i^{(2)''}, \quad \text{for } i = 1, 2 \quad (19)$$

$$\chi^{(3)} = \chi^{(3')} + i\chi^{(3)''}$$

If all other assumptions remain valid, we obtain instead of Eqn (18)

$$I_s \sim \left\{ \begin{array}{l} (\eta|\chi^{(3)}|^2 + \frac{2\eta\chi_1^{(2)'}\chi_2^{(2)'}\chi^{(3)'}\tau_p}{(\alpha_p/2)^2 + \tau_p^2} \\ (\gamma_2 - \delta\gamma_3) + \frac{[(\chi_1^{(2)'}\chi_2^{(2)'})^2]}{(\alpha_p/2)^2 + \tau_p^2} \\ \left[\gamma_2^2 + \delta^2 - \alpha_p\eta\frac{\chi^{(3)'}}{\chi_1^{(2)'}\chi_2^{(2)'}}(\gamma_2\gamma_3 + \delta) \right] \end{array} \right\} |f''(\Delta\mathbf{k})|^2 \quad (20)$$

where the following symbols are introduced for short:

$$\delta \equiv \frac{\chi_1^{(2)'}}{\chi_1^{(2)'}} - \frac{\chi_2^{(2)'}}{\chi_2^{(2)'}} \quad \gamma_2 \equiv 1 + \frac{\chi_1^{(2)'}}{\chi_1^{(2)'}} \frac{\chi_2^{(2)'}}{\chi_2^{(2)'}} \quad \gamma_3 \equiv \frac{\chi^{(3)'}}{\chi^{(3)'}} \quad (21)$$

Apparently, the main structure of Eqn (18) is preserved in Eqn (19). All the coefficients before the background, interference and cascaded terms are modified. However, not all of them depend on the wave mismatches. Thus, the angular lineshape of I_s , measured at a constant frequency, should retain the same character. In terms of the dependence on τ_p at a fixed $\Delta\mathbf{k}$, this consists of the constant background, the cascaded peak and the interference between them. Although the weighting factors of these three terms are changed, the position and width of the cascaded peak remain the same: the former is determined by the condition $|\mathbf{k}_1 - \mathbf{k}_2| = k_p = n_p\omega_p/c$ and the latter is equal to the polariton absorption α_p .

The cascaded peak loses its Lorentzian form when α_p becomes comparable to or greater than k_p , or when Eqn (14) is disturbed. Numerical calculations on the basis of Eqn (9) show that in these cases the bandwidth of the cascaded peak increases.

EXPERIMENTAL

We studied polaritons in a homogeneous crystal of LiIO_3 and crystals of LiNbO_3 doped with Mg and Nd. The dispersion properties of polaritons (the values of the real and imaginary polariton wavevectors, complex dielectric constants, refractive indices and polariton absorption coefficients) at the frequencies under consideration (corresponding wavenumbers were 741 cm^{-1} in the case of LiIO_3 and $530\text{--}570 \text{ cm}^{-1}$ in the case of the doped LiNbO_3) were known from the near-forward spontaneous Raman scattering data.¹⁶ The exciting pump waves 1 and 2 were generated by an Nd:YAG laser with a 20 ns pulse duration and a tunable LiF:F_2^- laser. The wavelength of the LiF:F_2^- laser can be tuned in the range $1.08\text{--}1.2 \mu\text{m}$. The second harmonic of the Nd:YAG laser was used as the probe pump. Three pumping beams were incident to the crystal at various angles (Fig. 1). The Stokes component of the scattered radiation was measured. Exciting pump 1 and the probe pump were e -polarized and exciting pump 2 was o -polarized in a crystal. Under these conditions the polarization of the polariton and signal waves in the crystals under investigation was ordinary. The linear dimensions of the scattering elements were of the order of 1 mm. All the conditions, taking into account the derivation of Eqn (20), were satisfied.

For each given polariton frequency, the corresponding frequencies of the tunable laser generation ω_2 and of the

signal under registration ω_s were set up as constant. To obtain the $I_s(\tau_p)$ dependence, we first measured the two-dimensional angle distribution of the signal intensity I_s . According to Eqn (18) or (20), I_s depends on the direct four-wave mismatch Δk and polariton wave mismatch τ_p . In turn, Δk and τ_p change with the angles of incidence of the three pumping beams. For changing Δk and τ_p over the whole necessary range, one has to scan any two angles of incidence of the pumping beams, or any two linear combinations of them. Our two-dimensional dependences consisted of series of curves $I_s(\alpha)|_{\theta_1}$. Each curve was measured under crystal rotation for the angle α , at different constant angles θ_1 between the first exciting pump and probe pump (Figs 1 and 2). The angle θ_2 between the second exciting pump and the probe pump was fixed. We then determined the cross-section of the two-dimensional $I_s(\theta_1, \alpha)$ dependence by the surface, where the mismatch for the direct four-wave interaction $\Delta k(\theta_1, \alpha)$ is equal to zero. In full agreement with the model predictions, each experimental curve $I_s(\alpha)|_{\theta_1}$ had a narrow maximum on this surface. The dependence of $\alpha_{\text{max}}(\theta_1)$ followed the condition $\Delta k(\theta_1, \alpha_{\text{max}}) = 0$. Thus, comparing theoretical predictions and experiment, we concluded from Eqn (17) that $I_s(\alpha_{\text{max}})|_{\theta_1} \sim |f''(0)|^2 I_s(\tau_p)$. In the second step, we calculated the polariton mismatch τ_p for each θ_1 and corresponding $\alpha_{\text{max}}(\theta_1)$. Finally, the desired lineshape $I_s(\tau_p)$ was plotted via $I_s = I_s(\alpha_{\text{max}})|_{\theta_1}$ as a function of $\tau_p = \tau_p[\theta_1, \alpha_{\text{max}}(\theta_1)]$.

We did not observe any constant background, caused by the direct scattering, in any of our experimental curves $I_s(\tau_p)$. This indicated that the effective components of third-order susceptibility were relatively small. The intensity dependences $I_s(\tau_p)$ obtained experimentally and by fitting the model expression given by Eqn (17) for LiIO_3 are shown in Fig. 3. Good agreement between the experiment and theoretical predictions was obtained. Both the position and the linewidth of the observed Lorentzian peak correspond to the values of the crystal parameters at the given polariton frequency.

However, in case of the crystals of $\text{LiNbO}_3:\text{Mg}$ and $\text{LiNbO}_3:\text{Mg}:\text{Nd}$ the experimental curves are much narrower than expected. It seems that their linewidths do

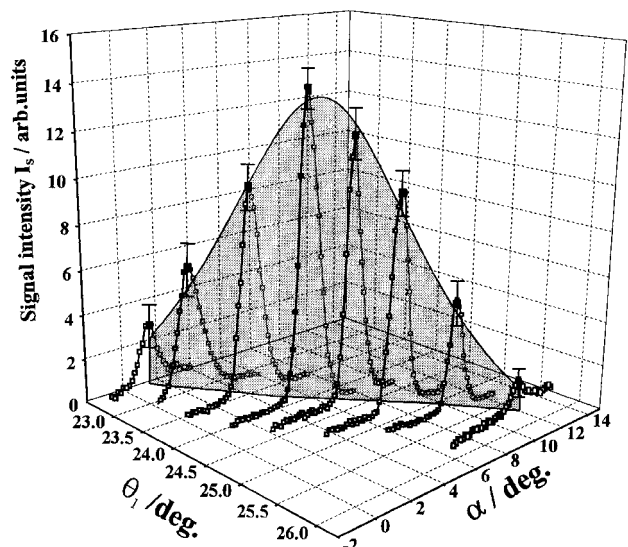


Figure 2. Signal intensity I_s as a function of polariton mismatch $I_s(\tau_p)$.

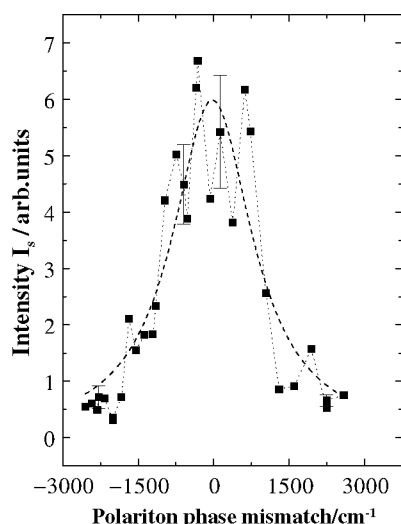


Figure 3. Signal intensity I_s as a function of polariton mismatch (dots, experiment; dashed curves, calculation) in a crystal of LiIO_3 (polariton wavenumber $\nu_p = 741 \text{ cm}^{-1}$, refractive index $n_p = 3.61$, absorption $\alpha_p = 1300 \text{ cm}^{-1}$).

not depend (or weakly depend) on the polariton absorption coefficient. Figure 4 shows examples of intensity dependences $I_s(\tau_p)$ for $\text{LiNbO}_3:\text{Mg}$ with different Mg concentrations C_{Mg} . In the case of the crystal with $C_{\text{Mg}} = 7.1 \text{ mol}\%$, the data were obtained for the polariton frequency inside the region where the dispersion of ϵ'_p has an anomalous character. The corresponding transverse phonon wavenumber is near 582 cm^{-1} . The expected values of the real and imaginary parts of the dielectric constant were calculated according to the data for near-forward scattering¹⁶ and dynamic parameters of E-type phonons¹⁷ (Fig. 5). Although the imaginary parts of the dielectric constant and polariton absorption coefficients are very high in this region, we observed a narrow polariton line with a well pronounced maximum.

At the same time, the positions of all observed maxima in $\text{LiNbO}_3:\text{Mg}$ and in $\text{LiNbO}_3:\text{Mg}:\text{Nd}$ were in good agreement with the expected values of the real part of the dielectric constant and polariton wavevector. The frequency dependences of the ordinary polariton

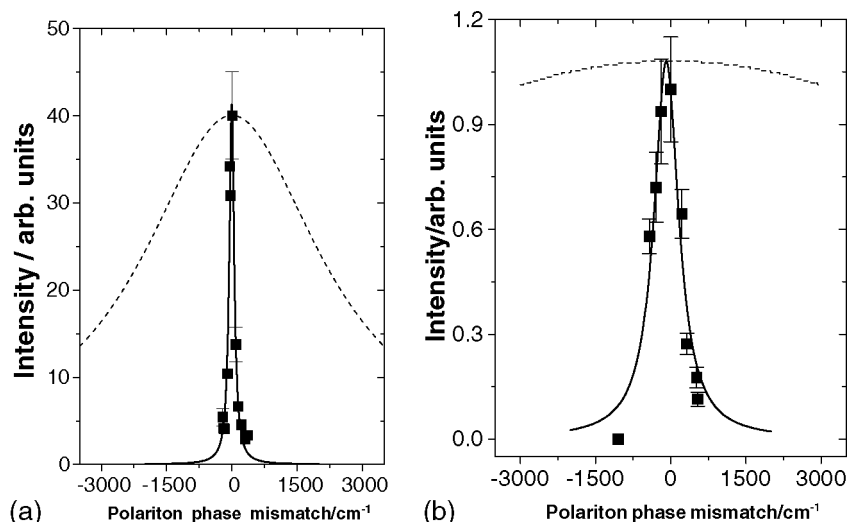


Figure 4. Signal intensity as a function of polariton mismatch (dots, experiment; dashed curves, calculation) in a crystal of $\text{LiNbO}_3:\text{Mg}$. (a) $C_{\text{Mg}} = 4.4 \text{ mol}\%$, polariton wavenumber $\nu_p = 541 \text{ cm}^{-1}$, $\alpha_p = 5000 \text{ cm}^{-1}$; (b) $C_{\text{Mg}} = 7.1 \text{ mol}\%$, $\nu_p = 575 \text{ cm}^{-1}$, $\alpha_p = 23000 \text{ cm}^{-1}$.

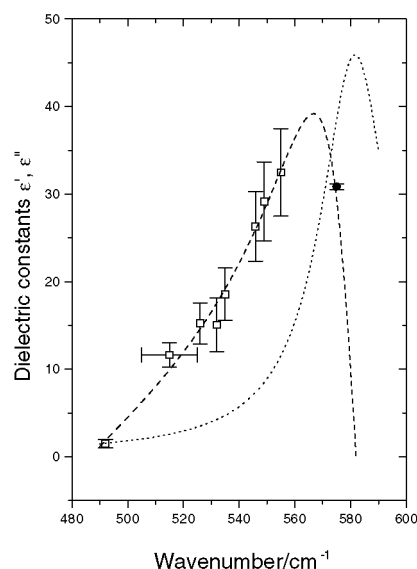


Figure 5. Dispersion of real (dashed curve) and imaginary (dotted curve, obtained by Burlakov *et al.*¹⁶) parts of the dielectric constant for ordinary waves in $\text{LiNbO}_3:\text{Mg}$ ($C_{\text{Mg}} = 7.1 \text{ mol}\%$). Squares, experimental data for spontaneous near-forward Raman scattering; circle, coherent cascaded scattering by the real part of the dielectric constant.

refractive index, measured by spontaneous scattering and by coherent four-wave scattering for one of the studied $\text{LiNbO}_3:\text{Mg}$, are given in Fig. 6.¹⁸ High coincidence can be seen. Note that the absolute error of the three-wave scattering data on refractive indices was approximately $\pm 0.2\text{--}0.5$, and the absolute error of the four-wave scattering data was smaller by an order of magnitude: $\pm 0.02\text{--}0.03$.

DISCUSSION

The theoretical consideration of four-wave coherent scattering was made on the basis of the conventional model. This model explained successfully different previous experiments with crystals of GaP ,⁵ GaAs ,⁶ LiIO_3 ⁸ and others. The only distinction between our description and the

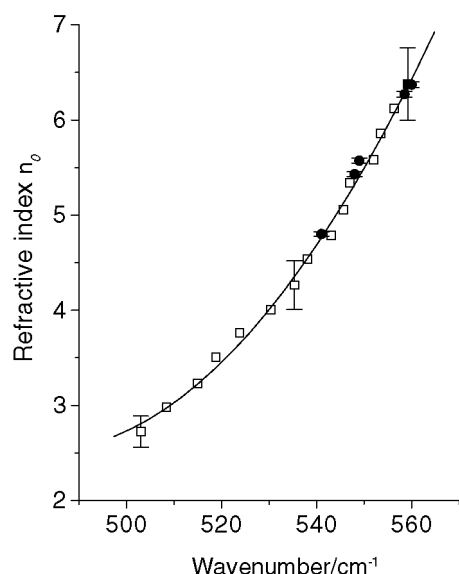


Figure 6. Dispersion of the ordinary refractive index of $\text{LiNbO}_3:\text{Mg}$ ($C_{\text{Mg}} = 4.4 \text{ mol\%}$) in the polariton range, obtained by spontaneous near-forward Raman scattering (squares) and coherent cascaded scattering (circles).

previous ones is the account for confined dimensions of the scattering element and the account of the imaginary parts of crystal non-linear susceptibilities in the vicinity of intrinsic resonances. With regard to the crystal of LiIO_3 , our experimental results confirm the validity of the theoretical model. However, the unusual narrowing of the intensity dependences $I_s(\tau_p)$ in the doped LiNbO_3 cannot be explained in the frame of the theoretical results obtained in this paper or earlier.

Unfortunately, we cannot give any convincing explanation of the observed angular dependences of the cascaded scattering in the doped LiNbO_3 . We cannot explain them by photorefractive properties of these crystals since the same narrowing effect exists in crystals with different Mg contents, before and after the photorefractive threshold at $C_{\text{Mg}} \approx 5 \text{ mol\%}$. It seems probable that the reason is connected with the resonance-type excitation of the crystal electronic states during the four-wave interaction in LiNbO_3 . First, the width of the electronic band gap in LiNbO_3 (near 3.8 eV^{19}) is much smaller than in LiIO_3 and less than the summary energy of two photons of the probe pump. The population of the electronic conductivity band can increase due to two-photon absorption effects. Next, the frequency ω_2 of the second exciting pump wave turns out to be in resonance with the polaronic states, the self-localized electrons at Nb ions of the crystal lattice.²⁰ Excitation of the electronic subsystem can lead to an increase in the effective value of $\chi_1^{(2)}$ and to a change in the probable interaction mechanism. If the

second-order susceptibility becomes sufficiently large, the process of stimulated generation of the polariton wave can occur. The necessary conditions take place when the parametric enhancement of the polariton wave prevails over the polariton damping relaxation. There can be another type of polariton generation, due to coherent relaxation of the electronic states through the simultaneously excited polaritons. In any case, the process of polariton generation can lead to narrowing of the polariton lineshape. However, the observed levels of I_s in LiNbO_3 are not much greater than that in LiIO_3 , where no generation narrowing exists. Nevertheless, the idea of the interaction between the certain electronic states and coherently excited polariton states seems to be interesting for further consideration.

Owing to the narrowing effect we lose the possibility of measuring the free polariton absorption in LiNbO_3 , but we can determine the polariton refractive index and dispersion of the real part of the wavevector with high accuracy. Figure 5 illustrates the ability to determine the dispersion characteristics in the vicinity of the phonon resonance.

CONCLUSION

The four-wave coherent cascaded scattering by polaritons proves to be a sensitive spectroscopy method. Owing to the high intensity of the coherent scattering, the signal-to-noise ratio can be much more than in case of the spontaneous near-forward Raman technique. This can be used in studying polaritons in small-sized objects, or for the measurement of the spatial distribution of polariton properties in inhomogeneous media. The descriptive theoretical treatment of this effect, made on the basis of the conventional model, accounting for the finite dimension of the scattering volume and the imaginary character of the non-linear susceptibilities, is appropriate for the exploration of polaritons in many non-linear crystals.

The question still remains of how to explain the narrowing of the angular distribution of the signal intensity in the Mg-doped crystals of LiNbO_3 . Owing to the narrowing effect, we lose the possibility of measuring of the free polariton absorption. However, we probably obtain the possibility of determining the polariton refractive index and dispersion of the real part of the wavevector with higher accuracy. Figure 5 illustrates the amazing ability to determine the dispersion characteristics in the direct vicinity of the phonon resonance.

Acknowledgments

The authors are grateful to I. I. Naumova for kindly supplying the $\text{LiNbO}_3:\text{Mg}$ and $\text{LiNbO}_3:\text{Mg}:\text{Nd}$ samples. This work was carried out in frames of the Russian Program 'Integration: Fundamental Optics and Spectroscopy' and was supported by the Russian Foundation for Basic Research (Grants 98-02-16877 and 99-02-16418).

REFERENCES

- Polivanov YN. *Sov. Phys. Usp.* 1978; **21**: 805.
- Loulergue JC, Etchepare J. *Phys. Rev. B* 1995; **52**: 15160.
- Bakker HJ, Hunsche S, Kurz H. *Rev. Mod. Phys.* 1998; **70**: 523.
- Akhmanov SA, Koroteyev NI. *Methods of Nonlinear Optics in Spectroscopy of Light Scattering*. Nauka: Moscow, 1981; 188.
- Coffinet JP, DeMartini F. *Phys. Rev. Lett.* 1969; **22**: 60.
- Yablonovitch E, Flytzanis C, Bloembergen N. *Phys. Rev. Lett.* 1972; **29**: 865.
- Wynne JJ. *Phys. Rev. Lett.* 1972; **29**: 650.
- Polivanov YuN, Sukhodolsky AT. *Sov. JETP Lett.* 1977; **25**: 221.
- Klyshko DN. *Sov. J. Quantum Electron.* 1975; **5**: 149.

10. Strizhevskii VL, Yashkir YuN. *Sov. J. Quantum Electron.* 1975; **5**: 541.
11. Vallee F, Flytzanis C. *Phys. Rev. B* 1992; **46**: 13799; *Phys. Rev. Lett.* 1995; **74**: 3281.
12. Qiu T, Maier M. *Phys. Rev. B* 1997; **56**: R5717.
13. Kitaeva GK, Mikhailovsky AA, Losevsky PS, Penin AN. *Opt. Commun.* 1997; **138**: 242.
14. Kitaeva GK, Mikhailovsky AA, Penin AN. *Sov. JETP* 1997; **85**: 1094.
15. Klyshko DN. *Photons and Non-linear Optics*. Gordon and Breach: New York, 1987.
16. Burlakov AV, Chekhova MV, Kulik SP, Penin AN. *Opt. Commun.* 1999; **165**: 39.
17. Barker AS, Loudon R. *Phys. Rev.* 1967; **158**: 433.
18. Kitaeva GK, Kuznetsov KA, Mikhailovsky AA, Naumova II, Penin AN. *Proc. SPIE* 1998; **3732**: 65.
19. Donnerberg H, Tomlinson SM, Catlow CRA, Schirmer OF. *Phys. Rev. B* 1989; **40**: 11909.
20. Schirmer OF, Thiemann O, Wohlecke M. *J. Phys. Chem. Solids* 1991; **52**: 185.